Tectonophysics 818 (2021) 229074

Contents lists available at ScienceDirect

Tectonophysics

journal homepage: www.elsevier.com/locate/tecto

Formation mechanism of the North–South Gravity Lineament in eastern China

Yangfan Deng [a,b,*], Yi-Gang Xu [a,b,*], Yun Chen [b,c,*]

[a] State Key Laboratory of Isotope Geochemistry, Guangzhou Institute of Geochemistry, Chinese Academy of Sciences, Guangzhou 510640, China
[b] CAS Center for Excellence in Deep Earth Science, Guangzhou 510640, China
[c] State Key Laboratory of Lithospheric Evolution, Institute of Geology and Geophysics, Chinese Academy of Sciences, Beijing 100029, China

ARTICLE INFO

Keywords:
North–South Gravity Lineament
Crustal thickness
Crustal density
Lithospheric density
Mantle transition zone structure
Gravity modeling

ABSTRACT

Gravity lineaments are well recognized along plate boundaries and in the interiors of oceanic plates. However, the formation mechanism of intracontinental gravity lineaments remains poorly understood. The North–South Gravity Lineament (NSGL), which extends >4000 km from Russia to South China, is characterized by an abrupt change in the observed Bouguer gravity anomaly, ranging from −100 mGal in the west to −40 mGal in the east over a distance of <100 km. Here we employ gravity modeling along a deep seismic sounding profile that transects the NSGL to delineate the relative contributions of the thickness and composition of the crustal and upper mantle and the stagnant slab in the mantle transition zone to the observed gravity anomaly, and to ultimately constrain the formation mechanism of the NSGL. Our results indicate that crustal thickness is the dominant factor in the formation of the NSGL, with lithospheric composition also playing a role. Combining our results with those of previous studies, lateral variations in the lithospheric mantle composition and crustal/lithospheric thickness across the NSGL can be attributed to lithospheric thinning and mantle replacement in the eastern part of the North China Craton during the late Mesozoic. This was triggered by the subduction of the Paleo-Pacific plate and subsequently led to the persistence of a stagnant slab and big mantle wedge. This study highlights the fundamental need for integrated geophysical–petrological analyses to better understand the surface response to deep tectonic processes.

1. Introduction

Gravity lineaments are typical features along plate boundaries and in the interiors of oceanic plates, aligning either roughly parallel or perpendicular to the direction of plate motion. They can form via either small-scale convection, slow and diffuse lithospheric extension, downward cooling of the lithosphere (thermal contraction), or viscous fingering instabilities (e.g., Cormier et al., 2011). Conversely, intracontinental gravity lineaments are poorly characterized, and their formation mechanism remains unclear. Therefore, it is necessary to assess the models proposed for oceanic lineaments to determine if they are applicable to their counterparts in continental settings.

The North–South Gravity Lineament (NSGL; also known as the Great Xing'an–Taihangshan Gravity Lineament) is a ~ 4000-km-long, ~100-km-wide zone in eastern China. It extends from Russia to South China and possesses a Bouguer gravity anomaly that decreases rapidly from −100 mGal in the west to −40 mGal in the east. Considerable changes in the surface elevation, crustal and lithospheric thickness, and potentially the structure of the mantle transition zone (MTZ) have been observed across this gravity lineament (Ma, 1989; Niu, 2005; Xu, 2007; Deng and Levandowski, 2018; Fig. 1). Such lateral heterogeneities have been attributed to the diachronous destruction of the North China Craton (NCC) during the Early Cretaceous (Xu, 2007). The NSGL is considered the western boundary of the destroyed NCC (Chen, 2010; Zhu et al., 2012b), and its position is potentially governed by vigorous mantle convection that was induced by the subduction of the Paleo-Pacific plate beneath the Eurasian plate (Zhao et al., 2004; Xu, 2007; Lei and Zhao, 2005; Zhao et al., 2007).

This study explores the conceptual model for the formation of the NSGL in detail via gravity modeling along a deep seismic sounding profile. First, we undertake a comprehensive compilation and analysis of the available gravity data to better characterize the NSGL in terms of regional heat flow, volcanism, and lithospheric architecture. We then assess the relative contributions of the crustal thickness, crustal and

* Corresponding authors at: CAS Center for Excellence in Deep Earth Science, Guangzhou 510640, China.
E-mail addresses: yangfandeng@gig.ac.cn (Y. Deng), yigangxu@gig.ac.cn (Y.-G. Xu), yunchen@mail.iggcas.ac.cn (Y. Chen).

https://doi.org/10.1016/j.tecto.2021.229074
Received 27 May 2021; Received in revised form 19 September 2021; Accepted 20 September 2021
Available online 25 September 2021

upper mantle compositions, and stagnant slab within the MTZ to the formation of the NSGL. Finally, we use the results of this NSGL investigation to place constraints on the formation of intracontinental gravity lineaments and discuss the implications of deep tectonic processes being able to produce such a large-scale geological feature.

2. Gravity data and characteristics of the NSGL

The NSGL is characterized by a rapid and distinct change in the Bouguer gravity anomaly across eastern China (Fig. 1). The Bouguer gravity data are from the Earth Gravitational Model (EGM2008), which spans land and ocean areas at a 2.5 × 2.5 arcmin grid spacing. The standard deviation of the Bouguer gravity data in this area is < 5 mGal (Pavlis et al., 2012). The Bouguer gravity that span the −100- to −40-mGal range are highlighted in Fig. 1 to illustrate the NGSL. The NGSL is particularly narrow within the NCC, possessing a minimum width of <50 km, and becomes wide and diffuse in the northern part of Northeast China and central South China (>600 km), with these broader regions corresponding to gentle topographic variations.

This newly defined gravity anomaly map and a number of tectonic parameters along the NSGL are shown in Figs. 1 and 2, respectively. From Northeast China to South China, the NSGL runs approximately along Great Xing'an Range and transects the Yanshan, Taihangshan, and Qinling–Dabie orogens and Wulingshan (Fig. 1), separating the ~100 m elevation region to the east from the ~1 km elevation region to the west (Fig. 1b).

There is a significant change in crustal thickness across the NSGL (Fig. 2a; Fig. 8 in Zhang et al., 2020). The crustal thickness exceeds 35 km to the west of the NSGL, with the thickest crust (~50 km) occurring in South Qinling. Conversely, the crust to the east of the NSGL is characterized by a 30–35 km crustal thickness, with the crust thinning to <30 km beneath the Songliao and Bohai basins and the Cathaysia block. The lithosphere exhibits similar lateral thickness variations, with a thinner lithosphere observed to the east of the NSGL than the west (Deng and Levandowski, 2018; Fig. 2b).

The geographic location of the NSGL is roughly coincident with the western end of the stagnant slab in the MTZ, which has been detected via seismic tomography (Fig. 2c; Huang and Zhao, 2006; Chen and Pei, 2010; Wei et al., 2015; Liu et al., 2017; Huang et al., 2021). However, recent receiver function analyses have not detected visible variations in the MTZ thickness across the NSGL (Liu et al., 2015a, Sun et al., 2020; Han et al., 2020; Vinnik et al., 2020). Nevertheless, Datong and Changbaishan volcanoes are underlain by a relatively thick MTZ, thereby suggesting the potential for a high-water content in the MTZ (Sun et al., 2020; Wang et al., 2020).

The NSGL has a lower heat flow than the surrounding area. Specifically, the surface heat flow is higher to the east of the NSGL than it is to the west (Fig. 2d). However, intraplate volcanism occurs on both sides of the NSGL, especially in North and Northeast China (e.g., Datong, Honggeertu, Changbaishan, Jingbohu, Longgang, Arshan-Chaihe, and Wudalianchi–Keluo volcanoes). The NSGL and the surrounding region possess focused centers of Quaternary (and particularly Holocene) volcanism.

All of these features collectively suggest that the NSGL is not only a topographical boundary, but also a tectonic boundary that separates two tectonically distinct domains. Constraints on the formation mechanism of such a large-scale geological feature are necessary to advance our understanding of the regional geology of the eastern Asian continent

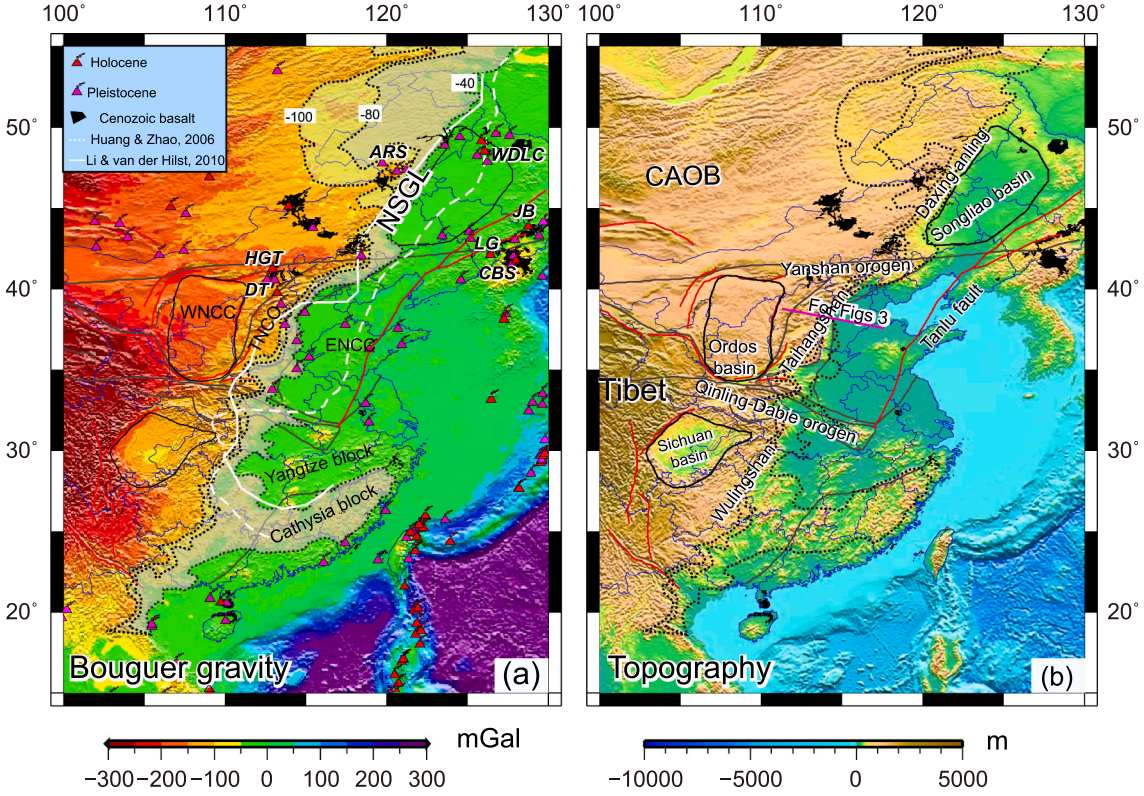

Fig. 1. Bouguer gravity anomaly (EGM2008, Pavlis et al., 2012) and topography (Etopo1, www.ngdc.noaa.goc/mgg/global/global.html) in eastern China. The white lines indicate the western boundary of stagnant slab from tomography (dash line: Huang and Zhao, 2006; solid line: Li and van der Hilst, 2010). Basalts and volcanos are outlined with black contours and triangles, respectively. Gravity contours of −100 mGal ~ −40 mGal or – 80 mGal ~ −40 mGal are marked in order to illustrate the feature of the NGSL. The purple line outlines the seismic profile in Fig. 3. CAOB: Central-Asian Orogen Belt; WNCC: Western North China Craton; ENCC: Eastern North China Craton; TNCO: Trans-North China Orogen. DT: Datong volcano; HGT: Honggeertu volcano; CBS: Changbaishan volcano; JB: Jingbo volcano; LG: Longgang volcano; ARS: Arshan volcano; WDLC: Wudalianchi volcano. The extent of NSGL is narrow in North China compared with that in Northeastern China and South China. (For interpretation of the references to colour in this figure legend, the reader is referred to the web version of this article.)

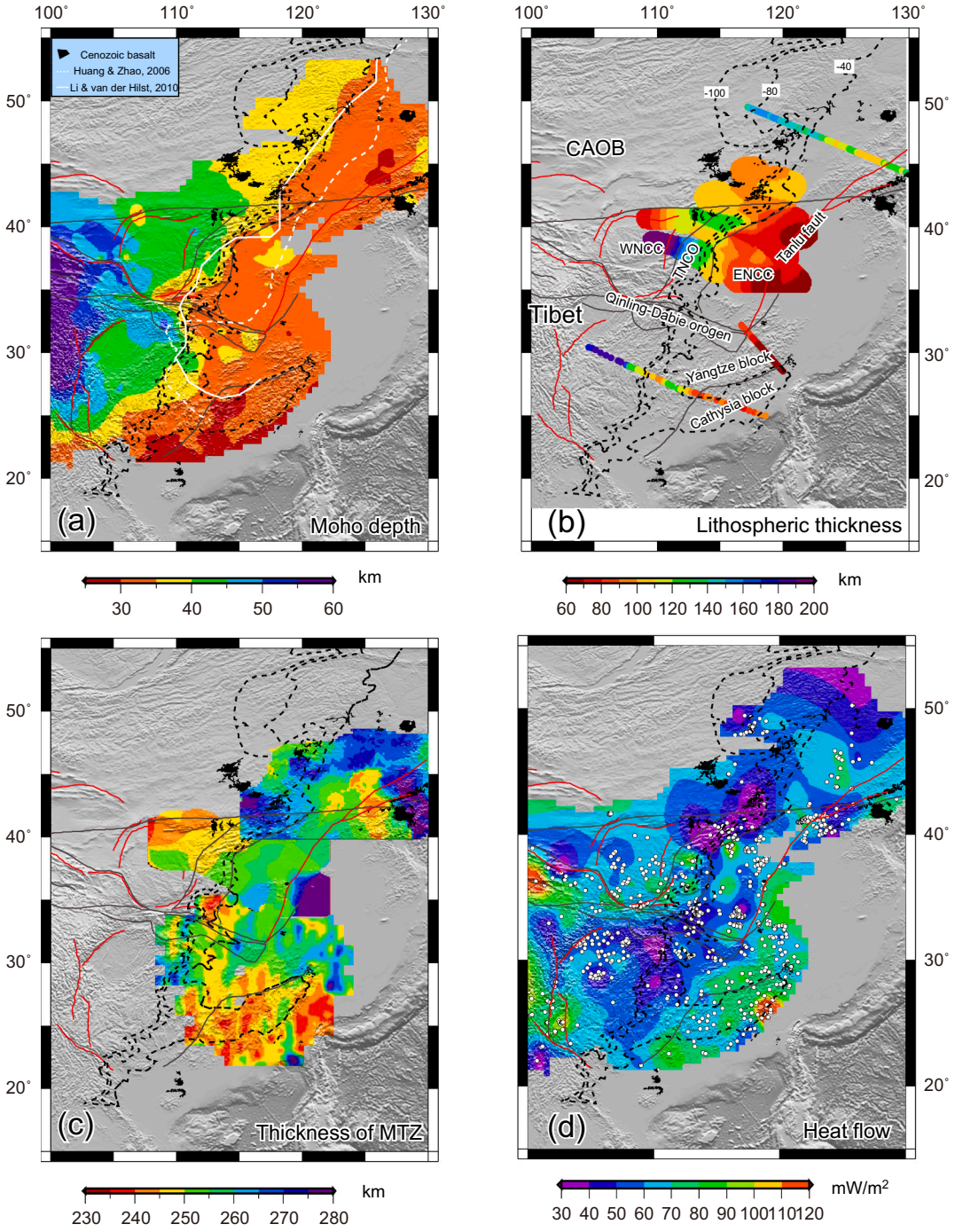

Fig. 2. The characteristics of the NSGL and its vicinity. (a) Crustal thickness (Li et al., 2014); (b) Lithospheric thickness from seismological results (Chen et al., 2009; Zheng et al., 2014; Zhang et al., 2014, 2018); (c) Thickness of mantle transition zone (North China: Chen et al., 2009; Northeast China: Liu et al., 2015a; South China: Han et al., 2020); The white dots indicate the locations for peridotites xenoliths. (d) Surface heat flow (Jiang et al., 2019). The white circles indicate the observation points; Gravity contours of −100 mGal, −80 mGal and –40 mGal are outlined with dotted lines. The meaning of white lines in (a) is the same as Fig. 1a.

and, more importantly, to elucidate the surface response to deep tectonic processes. Here we evaluate the potential factors responsible for the formation of the NSGL. This evaluation is focused on the NCC because: (a) the gravity lineament in this region is narrow, with distinct sedimentary, crustal, and lithospheric thickness contrasts observed across the NSGL, whereas those in South and Northeast China are broader; (b) previous studies have conducted extensive analyses of mantle xenoliths from both sides of the NSGL (e.g., Zheng et al., 2007); and (c) a deep seismic sounding profile spanning the NCC is available (Jia et al., 2014; Tian et al., 2014; Wang et al., 2014), thereby providing valuable information for gravity modeling.

3. Factors that may contribute to the formation of the NSGL

3.1. Gravitational contribution from Moho depth variations

There are significant variations in the crustal thickness across the NSGL, as shown in Fig. 2a and the seismic profiling results of Jia et al. (2014) and Tian et al. (2014), which have a profound effect on the observed gravity anomaly. Polygonal prisms are employed to calculate

the gravity anomaly due to the Moho depth variations (Jia and Meng, 2009), with a density contrast of 0.4 g/cm^3 applied between the lower crust and upper mantle (Mooney and Kaban, 2010). The crustal thickness undulations yield a similar gravity gradient to that observed across the NSGL, as shown in Fig. 3a. The crustal thickness is therefore considered to be the predominant factor driving the formation of the NSGL.

3.2. Gravitational contribution from intra-crust

Crustal interfaces and composition (including sediments) may also contribute to the formation of the NSGL. We calculated the density structure of the crust based on the detailed crustal compressional-wave velocity (Vp) structure on both sides of the NSGL using the seismic profiling results of Jia et al. (2014). The applied Vp model is slightly different from that of Tian et al. (2014), with a higher velocity employed in the lower crust, especially beneath the Ordos basin.

The crustal density (ρ) is derived from Vp as (Brocher, 2005):

$$\rho = 1.6612*v_p - 0.4721*v_p{}^2 + 0.0671*v_p{}^3 - 0.0043*v_p{}^4 + 0.000106*v_p{}^5 \quad (1)$$

and is then employed to calculate the gravity anomaly. The density in the mantle is assumed to be homogeneous (3.3 g/cm^3), since only the crustal contribution is considered here. Fig. 3b shows the density structure and corresponding gravity anomaly along the profile. The largest difference between the calculated and observed gravity anomalies is >50 mGal. The calculated gravity to the east of the NSGL is lower than the observed gravity, with the opposite trend observed to the west.

We could fit the observed gravity anomaly by assuming that the gravity difference originated within the crust and increasing (decreasing) the crustal density by 0.1 g/cm^3 on the eastern (western)

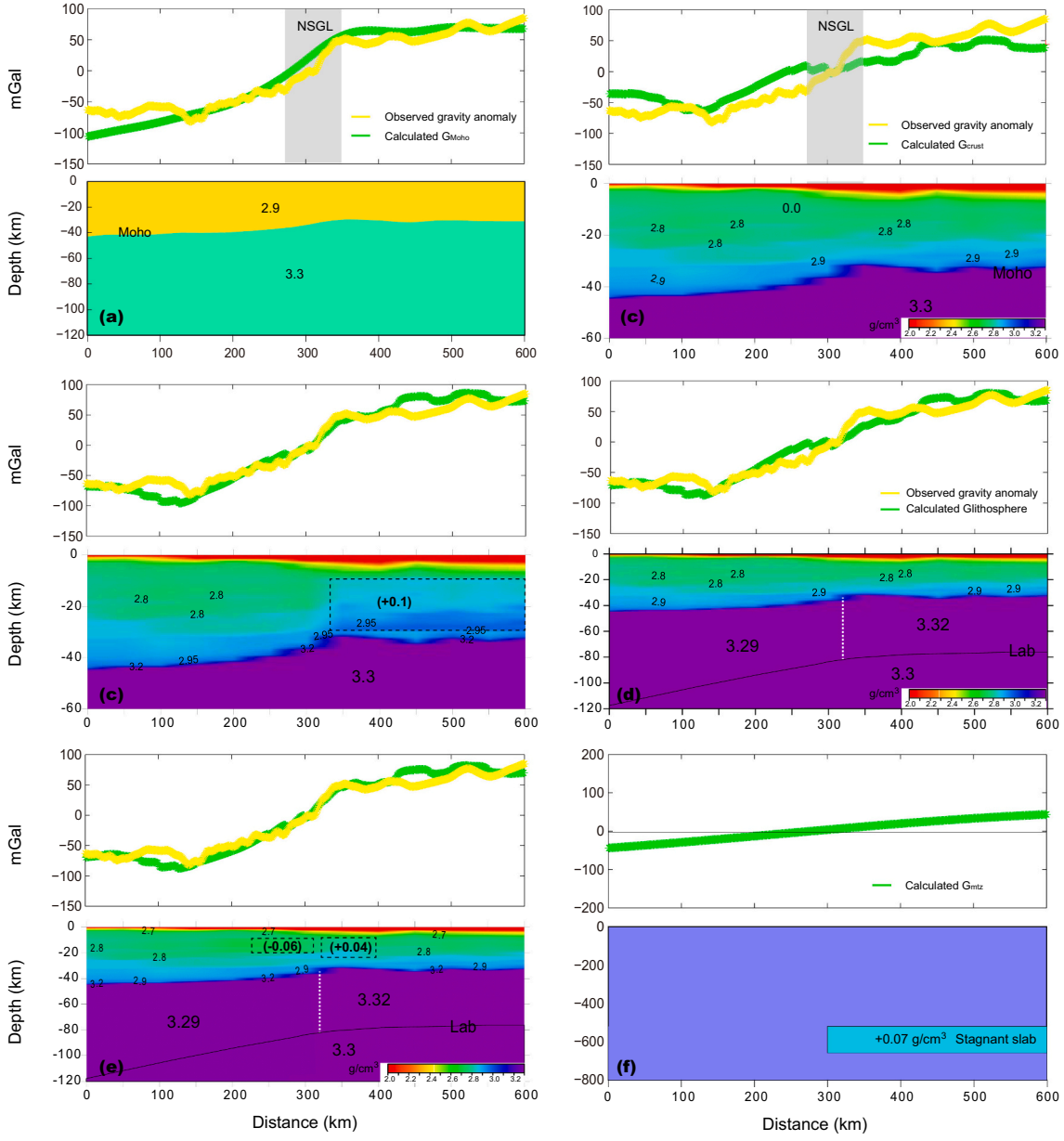

Fig. 3. Modeled gravity anomalies against the *E*-W deep seismic sounding profile shown in Fig. 1. Gravitational effects of (a) the Moho variation; (b) the crustal density from Vp; (c) the density model from (b) and + 0.1 g/cm3 in the dashed box; (d) the lithospheric density. The crustal density is the same as (b), the density in the mantle lithosphere is higher (+0.03 g/cm3) in the east side (The dashed white line is the boundary for the density difference); (e) the density model from (d) and + 0.04 g/cm3 density in the east side box and − 0.06 g/cm3 in the west side box of NSGL; (f) the stagnant slab. The means of anomalies have been removed.

side of the NSGL (Figs. 3c, S1a, and S1b). This density contrast could be derived from either 1) the Vp–ρ empirical relationship or 2) the wrong original Vp data. The Vp–ρ relationship in Brocher (2005) is widely applied, but the governing mechanism for this relationship is still unknown, especially when a particular rock type is considered. Furthermore, the uncertainties associated with this Vp–ρ relationship have not been directly assessed to date (Herceg et al., 2016). The crustal Vp to the east of the NSGL may be higher than that to the west. However, a passive seismic profile in the same region indicates that the shear-wave velocity structure of the crust to the east of the NSGL is lower than that to the west (Zheng et al., 2005). Furthermore, another model that used the same raw seismograms shows a higher velocity to the west (Tian et al., 2014) that contradicts the gravity modeling results of a higher density to the east side of the NSGL. Even though the higher crustal density to the east of the NSGL could provide a better fit to the gravity observations (Fig. 3c) than the crustal density structure in Fig. 3b, it is hard to explain the systematic density difference across the NSGL.

3.3. Gravitational contribution from the upper mantle

Another possibility for the observed gravity difference across the NSGL in Fig. 3b may be related to structural variations in the upper mantle. The lithospheric mantle in the eastern NCC (ENCC) is estimated to be ~50 °C colder than that beneath the western NCC (WNCC) at a given depth (the Moho temperature of the ENCC is 100 °C colder than that of the WNCC; Sun et al., 2013). Such a temperature difference indicates that the higher lithospheric velocity and density beneath the ENCC, which corresponds to a density increase of ~5 kg/m^3, is due to the colder temperature beneath the ENCC (assuming a thermal expansion coefficient of ~3.0 × 10^{-5}/°C; McKenzie et al., 2005). The upper mantle composition exerts a more significant influence on the mantle density than its temperature. Iron, volatiles, and aluminous phases, such as garnet and spinel, are preferentially extracted from the mantle during partial melting, leaving a drier mantle composition that is rich in magnesium; the opposite compositional trends are envisaged during fertilization processes. Empirical relationships between Mg# (Mg# = [Mg]/[Mg + Fe]), Vp, and ρ suggest that a unit increase in Mg# corresponds to a density decrease of ~0.4% (~13 kg/m^3; Schutt and Lesher, 2010). Previous studies of peridotite xenoliths have documented the differences in Mg# between the mantle beneath the central NCC and the ENCC (Polat et al., 2006; Zheng et al., 2007; Xu et al., 2008; Xu et al., 2010a, 2010b; Deng et al., 2013; Guo et al., 2016; Zhang et al., 2017). The Mg# in the central NCC mantle is ~2 units higher than that in the ENCC (Fig. 4), which indicates that the lithospheric mantle density to the east of NSGL is ~0.025 g/cm^3 higher than that to the west. We set the crustal density to the same crustal density structure in Fig. 3b and the asthenospheric density to 3.3 g/cm^3. The lithospheric thickness is taken from Wang et al. (2014), and the modeled lithospheric mantle density beneath the ENCC is higher (approximately +0.03 g/cm^3) than that beneath the WNCC (Fig. 3c).

The density anomaly in the lithospheric mantle (Fig. 3d) alone cannot produce the observed NSGL gravity pattern; however, a similar trend is witnessed between modeled and observed gravity anomalies (Fig. 3d). Furthermore, if we assume that local density anomalies are present in the crust (Figs. 3e, S1c, and S1d), then the calculated gravity pattern fits the observed NSGL gravity pattern well. Local density anomalies are not required in the regions that possess smaller gravity anomaly variations across the NSGL. We therefore speculate that the Moho variations are primarily responsible for the lateral variations in the gravity anomaly across the NSGL, whereas the lithospheric density differences exert a secondary influence on the observed gravity anomaly.

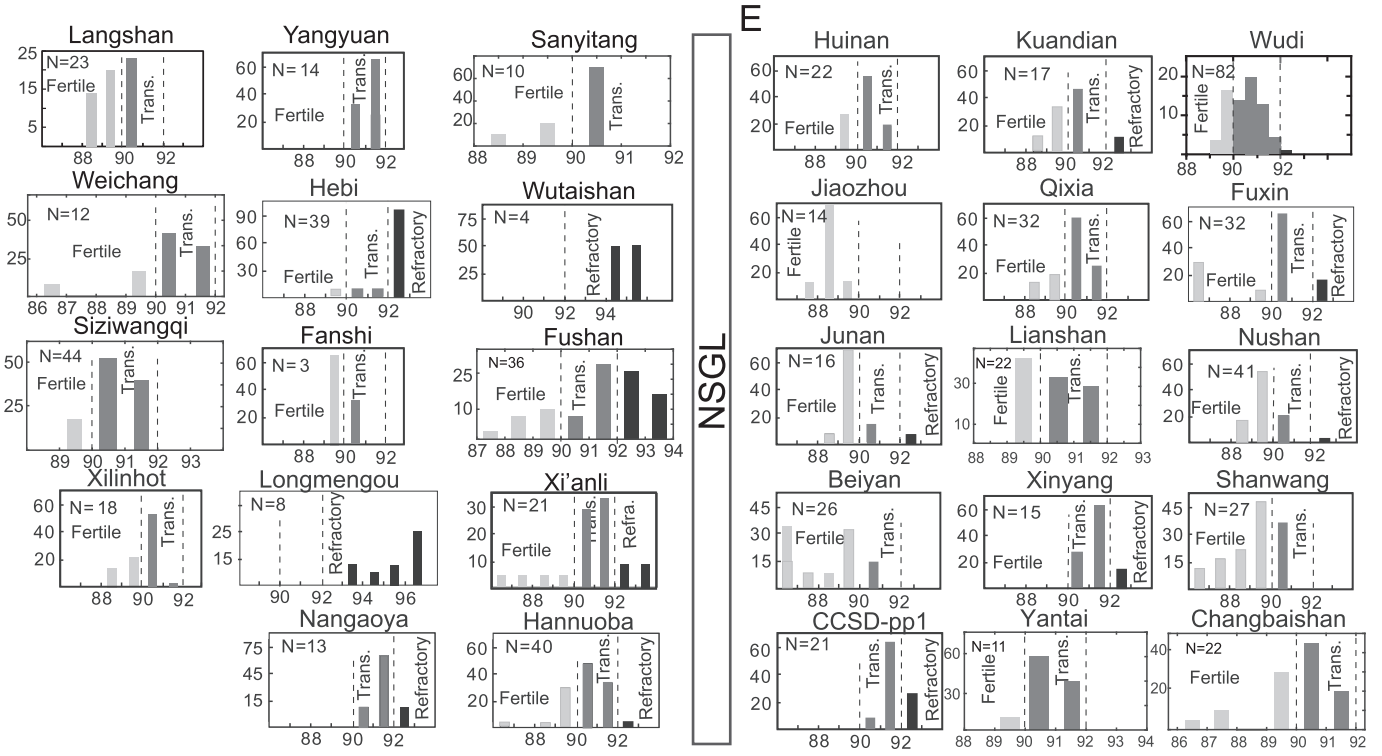

Fig. 4. Distribution of olivine-Mg# in peridotites on the sides of NSGL: Fertile, olivine-Mg# < 90; Transitional (Trans.), olivine-Mg# 90–92; Refractory (Refra.), olivine-Mg# > 92. Data sources: Wutaishan: Polat et al., 2006; Yangyuan, Fanshi: Xu et al., 2008; Fushan: Xu et al., 2010a; Xi'anli: Xu et al., 2010b; Beiyan: Xiao et al., 2010; Yantai: Hong et al., 2012; Xilinhot: Pan et al., 2013; Wudi: Liu et al., 2015b; Weichang: Zou et al., 2016; Longmengou: Zhang et al., 2017. Langshan: Dai et al., 2019; Lianshan: Hao et al., 2019; Changbaishan: Xu et al., 2019; Nangaoya: Bian et al., 2021; Siziwangqi: Zhang et al., 2021; Sanyitang: Zhao et al., 2021; other details can be seen in Zheng et al. (2007). The Y-axis indicates the frequency. The locations of the peridotites xenoliths are shown in Fig. 2c.

3.4. Gravitational contribution from the stagnant slab in the mantle transition zone

The effect of the stagnant slab in the MTZ on the overlying lithosphere and intraplate volcanism in East Asia is popular research topic (Zhao et al., 2004; Fukao et al., 2009; Xu et al., 2018). Given the geographic proximity of the western end of the stagnant slab in the MTZ and the NSGL (Huang and Zhao, 2006; Chen and Pei, 2010; Chen, 2010), it has been proposed that the stagnant slab may have induced vigorous mantle convection, thus affecting the composition and structure of the shallow lithosphere (Xu, 2007; Ohtani and Zhao, 2009) and volcanism (Zhao et al., 2004; Kuritani et al., 2011; Xu et al., 2012; Wang et al., 2017) across the NSGL. The density contrast between the western Pacific slab and the mantle beneath the Japan trench is assumed to be constant at 0.07 g/cm^3 (Furuse and Kono, 2003; Faccenna et al., 2012), and the thickness of the stagnant slab is 140 km based on triplication waveform modeling (Li et al., 2013). Fig. 3f presents the calculated gravity anomaly when a slab is present in the MTZ, with an east-to-west increasing gravity anomaly that is similar to that observed for the NSGL, but with a much longer wavelength. We therefore suggest that the gravity anomaly from a stagnant slab is a negligible contributor to the observe NSGL gravity pattern because the near-neutral buoyancy of the slab due to the low-density phases may be offset by the lower temperatures (King et al., 2015).

4. Discussion

4.1. Lateral variations in the gravity anomaly across the NSGL due to the destruction of the ENCC

The modeling presented in this study demonstrates that the lateral variations in the gravity anomaly across the NSGL are due primarily to crustal thickness variations and secondarily to contrasting lithospheric compositions across the NSGL. Specifically, the thicker crust and more refractory upper mantle beneath the TNCO relative to those beneath the ENCC explain the gravity anomaly gradients across the NSGL. Therefore, the processes that created these E–W lateral variations in mantle composition and crustal thickness were responsible for the formation of the NSGL, with the partial destruction of the NCC being the most likely formation mechanism (Menzies et al., 1993; Griffin et al., 1998; Xu, 2001).

Considerable changes in lithospheric thickness and mantle composition have been documented to the east of the NSGL. Ordovician diamondiferous kimberlites and their mantle xenoliths indicate a thick (>180 km), ancient (>2.5 Ga), cold, refractory lithospheric keel beneath the ENCC prior to the Paleozoic, whereas Cenozoic alkali basalts and their hosted xenoliths, and geophysical investigations, reveal the presence of a thin (~80 km), hot, fertile lithosphere (Menzies et al., 1993; Griffin et al., 1998; Xu, 2001; Gao et al., 2002; Chen, 2010). Such a dramatic change in lithospheric architecture is now known as cratonic destruction, and most likely took place during the late Mesozoic (Zhu et al., 2012b). The ENCC experienced significant lithospheric extension and thinning during this cratonic destruction, and its original refractory cratonic root (higher Mg#) was replaced by a relatively fertile mantle (lower Mg#) via either thermal erosion and subsequent accretion or melt–rock interactions (Xu, 2001; Zhang, 2005; Zheng et al., 2007; Wu et al., 2008). This lithospheric destruction is confined largely to east of the NSGL, leaving the WNCC largely intact, and therefore creating a significant mantle density/composition contrast across the NSGL. A paleogeographic reconstruction (Wang, 1985) further supports the destruction of the NCC as the formation mechanism of the NSGL, whereby the NSGL first appeared during the Early Cretaceous, which coincides with the peak period of destruction of the NCC (Xu, 2007).

The crustal thickness exerts a primary influence on the gravity anomaly, as shown in Fig. 3. The Moho is ~45 km thick to the west of the NSGL, whereas it is only ~35 km thick to the east. Similarly, the lithosphere is ~140 km thick to the west of the NSGL and ~ 80 km thick to the east (Fig. 2). However, the mechanism driving this west-to-east crustal thinning remains unclear, with lithospheric stretching and gravitational instability of the dense lower crust being the two main candidates to explain this thinning. A recent compilation shows that the (disturbed) ENCC and (intact) WNCC possess virtually identical physical structures and compositions (a thin mafic lower crust and predominantly intermediate composition overall), although the crust in the disturbed region is thinner than that in the intact craton (Ma et al., 2019). This suggests that delamination of the lower crust was not a viable mechanism for thinning the crust beneath the ENCC. This crustal thinning may be related to simple lithospheric stretching during the late Mesozoic, as evidenced by basin formation and the emplacement of metamorphic core complexes (Zhu et al., 2012a). Furthermore, the thinning ratios for the crust and lithosphere are ~0.2 and ~ 0.4, respectively, which are consistent with a pure shear model and lithospheric detachment/delamination in this region.

4.2. Paleo-Pacific plate subduction, big mantle wedge, and the North–South Gravity Lineament

Although the destruction of the ENCC provides a viable mechanism to generate the E–W variations in the gravity anomaly across the NSGL, it fails to fully account for the formation of the NSGL because the lineament spans almost the entirety of eastern China, even extending to Russia, rather than being confined to North China. The deep tectonic processes that triggered the destruction of the ENCC may be the most plausible driver. The subduction of the Pacific plate beneath the Asian continent is now considered the main trigger for the destruction of the NCC (Zhu et al., 2012b) because of the following: (a) the spatial pattern of cratonic destruction (approximately NE–SW-oriented extensional basins, main structural alignments, and metamorphic core complexes) is consistent with the subduction direction of the Pacific plate (Zhu et al., 2012a); (b) two main episodes of late Mesozoic magmatism have been identified (Jurassic and Early Cretaceous), which correspond to the subduction of the Pacific plate beneath the Eurasian plate and subsequent extensional episodes, respectively (Wu et al., 2019; Ma and Xu, 2021); and (c) seismic tomography studies have indicated that the subducted Pacific oceanic slab has become stagnant within the MTZ, and extends westward subhorizontally beneath the eastern Asian continent (Zhao et al., 2004; Huang and Zhao, 2006; Huang et al., 2021). The westernmost end of this stagnant slab does not extend beyond the NNE–SSW-trending NSGL (Xu, 2007). Such a configuration outlines an ultimate link between Pacific plate subduction and cratonic destruction; the NSGL represents the western boundary of the destroyed NCC.

Fig. 5 schematically illustrates the scenario for the formation of the NSGL in East Asia, whereby subduction of the Paleo-Pacific plate led to the formation of the big mantle wedge (BMW) beneath the eastern Asian continent (Zhao et al., 2004; Lei and Zhao, 2005; Zhao et al., 2007; Ohtani and Zhao, 2009; Lei, 2012; Xu et al., 2018), and the dehydration and decarbonization of the stored slab in the MTZ released volatiles into the upper mantle (Xia et al., 2019). The ingression of volatiles, including water and CO_2, would considerably weaken the lithosphere, and would therefore be responsible for the general lithospheric thinning trend beneath the eastern Asian continent; the destruction of the NCC would be one of the major manifestations of this lithospheric thinning (Niu, 2005; Xu, 2007; Li et al., 2016, 2019; Sun et al., 2021).

Liu et al. (2017) have argued that the seismically detected stagnant slab in the MTZ is a recent feature that may be younger than 30–20 Ma. However, this does not preclude the possibility that the stagnant slab structure, which is also known as the BMW structure, may have existed since the Early Cretaceous. For example, Nishi et al. (2013) advocated that stagnant slabs may potentially persist in this region for >100 Myr owing to the slow rate of Si—Al interdiffusion. The constraints on such a persistent mantle structure can be also captured in the migration pattern of the late Mesozoic magmatism in the NCC (Kiminami and Imaoka,

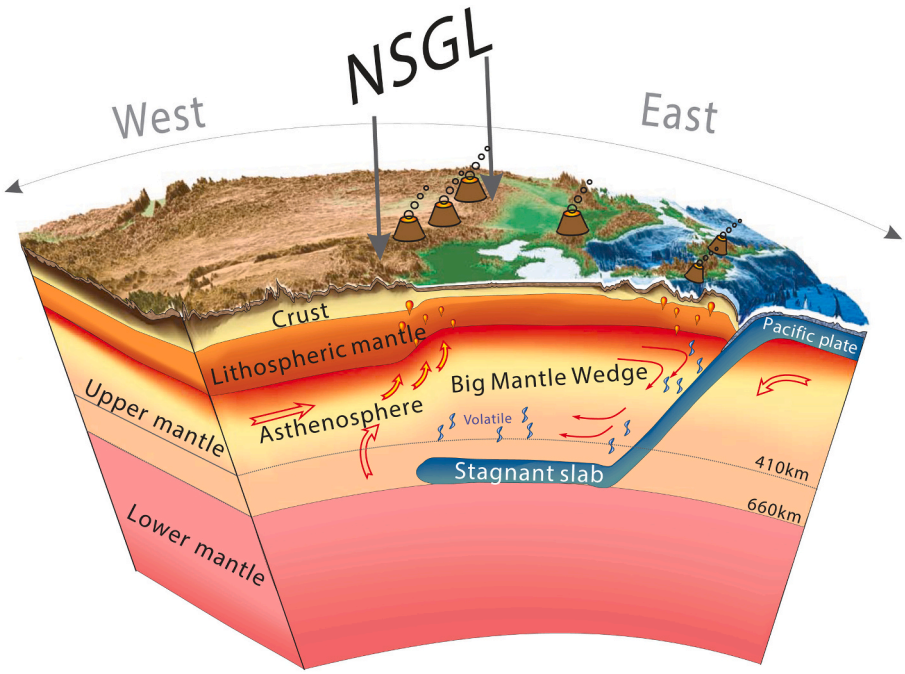

Fig. 5. A schematic diagram for the formation of NSGL in North China Craton. The stagnation of the subducted pacific slab within the MTZ created a BMW structure since the early Cretaceous (e.g., Zhao, 2004; Lei and Zhao, 2005; Zhao et al., 2007; Xu, 2007), in which vigorous convection and volatiles (including water and CO2) released from the stored slab would considerably weaken and thin the overlying lithosphere.

2013; Wu et al., 2019). Ma and Xu (2021) recently analyzed geochronological, whole-rock geochemical, and zircon Hf isotope data from Mesozoic magmas in the northern NCC, and their age-dating results revealed that a magmatic belt migrated >1000 km inland during 185–145 Ma and then back again after 145–140 Ma, coincident with the transition from compression to extension at the start of the Early Cretaceous. Such a feature is interpreted as being the consequence of a change in the geodynamic regime of the subducting Paleo-Pacific slab and its interaction with the overlying continental lithosphere, which involves an active continental arc that spanned the Korean and Liaodong peninsulas in the Early–Middle Jurassic, progressive shallowing of the subducting Paleo-Pacific plate in the Middle–Late Jurassic, and subsequent slab rollback in the Early Cretaceous. Since stagnation of the subducting slab in the MTZ is only possible when the subducting plate is retreating (Griffiths et al., 1995), this spatiotemporal magmatic pattern strongly suggests the persistence of the BMW structure beneath the eastern Asian continent since the Early Cretaceous, with this peculiar deep mantle structure governing the post-Cretaceous evolution of the Asian continental lithosphere by mediating the chemical and physical properties of the upper mantle. This observation therefore bolsters a potential link between the NSGL and Pacific plate subduction.

5. Conclusion

We investigated the origin of intracontinental gravity lineaments in the NSGL in eastern China by integrating geophysical and geochemical data. Gravitational contributions from Moho variations, crustal and upper mantle compositions, and the stagnant slab are evaluated, together with gravity modeling along a deep seismic profile. These integrated results indicate that the NSGL is caused primarily by variations in the Moho, with the contrasting lithospheric compositions on either side of the lineament having a secondary effect on the NSGL. The process responsible for the subduction of the Paleo-Pacific plate and subsequent destruction of the NCC was the ultimate driving force for the formation of the NSGL, since the lateral variations in crustal thickness and mantle composition across the NSGL are most likely related to the destruction of the ENCC. It is therefore proposed that stagnation of the subducted Pacific slab within the MTZ created a BMW structure that has persisted since the Early Cretaceous, such that vigorous convection and the volatiles released from the subducted slab have played important roles in re-shaping the shallow lithosphere.

Supplementary data to this article can be found online at https://doi.org/10.1016/j.tecto.2021.229074.

Declaration of Competing Interest

The authors declare that they have no known competing financial interests or personal relationships that could have appeared to influence the work reported in this paper.

Acknowledgements

The Bouguer gravity data were obtained from the website (https://bgi.obs-mip.fr/data-products/grids-and-models/egm2008-global-model/). The gravity modeling code is originated from Dr. Peng Wang. The authors benefited from helpful discussions with Dr. Qiang Ma. This research was supported by the Strategic Priority Research Program (B) of the Chinese Academy of Sciences (XDB18000000), National Science Foundation of China (41874106, 42021002), and Youth Innovation Promotion Association CAS (YIPA2018035).

References

Bian, X., Su, Y., Zheng, J., Xiong, Q., Zhou, X., Dai, H., et al., 2021. Multi-stage mantle accretions and metasomatisms related to peripheral subduction or collision in the northern North China Craton: evidence from the Nangaoya peridotite xenoliths. Lithos 390-391, 106116. https://doi.org/10.1016/j.lithos.2021.106116.

Brocher, T.M., 2005. Empirical relations between elastic wavespeeds and density in the Earth's crust. Bull. Seismol. Soc. Am. 95 (6), 2081–2092. https://doi.org/10.1785/0120050077.

Chen, L., 2010. Concordant structural variations from the surface to the base of the upper mantle in the North China Craton and its tectonic implications. Lithos 120, 96–115. https://doi.org/10.1016/j.lithos.2009.12.007.

Chen, L., Cheng, C., Wei, Z., 2009. Seismic evidence for significant lateral variations in lithospheric thickness beneath the central and western North China craton. Earth Planet. Sci. Lett. 286 (1), 171–183. https://doi.org/10.1016/j.epsl.2009.06.022.

Chen, Y.J., Pei, S., 2010. Tomographic structure of East Asia: II. Stagnant slab above 660 km discontinuity and its geodynamic implications. Earthq. Sci. 23 (6), 613–626. https://doi.org/10.1007/s11589-010-0760-4.
Cormier, M.-H., Gans, K.D., Wilson, D.S., 2011. Gravity lineaments of the Cocos Plate: evidence for a thermal contraction crack origin. Geochem. Geophys. Geosyst. 12 (7) https://doi.org/10.1029/2011GC003573.
Dai, H.-K., Zheng, J.-P., Xiong, Q., Su, Y.-P., Pan, S.-K., Ping, X.-Q., Zhou, X., 2019. Fertile lithospheric mantle underlying ancient continental crust beneath the northwestern North China craton: significant effect from the southward subduction of the Paleo–Asian Ocean. GSA Bull. 131 (1–2), 3–20. https://doi.org/10.1130/B31871.1.
Deng, Y., Levandowski, W., 2018. Lithospheric alteration, intraplate crustal deformation, and topography in eastern China. Tectonics 37 (11), 4120–4134. https://doi.org/10.1029/2018TC005079.
Deng, Y., Fan, W., Zhang, Z., Badal, J., 2013. Geophysical evidence on segmentation of the Tancheng-Lujiang fault and its implications on the lithosphere evolution in East China. J. Asian Earth Sci. 78, 263–276. https://doi.org/10.1016/j.jseaes.2012.11.006.
Faccenna, C., Becker, T.W., Lallemand, S., Steinberger, B., 2012. On the role of slab pull in the Cenozoic motion of the Pacific plate. Geophys. Res. Lett. 39, 136–149. https://doi.org/10.1029/2011GL050155.
Fukao, Y., Obayashi, M., Nakakuki, T., 2009. Stagnant slab: a review. Annu. Rev. Earth Planet. Sci. 37 (1), 19–46. https://doi.org/10.1146/annurev.earth.36.031207.124224.
Furuse, N., Kono, Y., 2003. Slab residual gravity anomaly: gravity reduction due to subducting plates beneath the Japanese Islands. J. Geodyn. 36, 497–514. https://doi.org/10.1016/S0264-3707(03)00062-0.
Gao, S., Rudnick, R.L., Carlson, R.W., McDonough, W.F., Liu, Y.-S., 2002. Re–Os evidence for replacement of ancient mantle lithosphere beneath the North China craton. Earth Planet. Sci. Lett. 198 (3), 307–322. https://doi.org/10.1016/S0012-821X(02)00489-2.
Griffin, W.L., Andi, Z., O'Reilly, S.Y., Ryan, C.G., 1998. Phanerozoic evolution of the lithosphere beneath the Sino-Korean Craton. Geodynamics Series 27, 107–126. https://doi.org/10.1029/GD027p0107.
Griffiths, R.W., Hackney, R.I., van der Hilst, R.D., 1995. A laboratory investigation of effects of trench migration on the descent of subducted slabs. Earth Planet. Sci. Lett. 133 (1), 1–17. https://doi.org/10.1016/0012-821X(95)00027-A.
Guo, Z., Afonso, J.C., Qashqai, M.T., Yang, Y., Chen, Y.J., 2016. Thermochemical structure of the North China craton from multi-observable probabilistic inversion: Extent and causes of cratonic lithosphere modification. Gondwana Res. 37, 252–265. https://doi.org/10.1016/j.gr.2016.07.002.
Han, R., Li, Q., Huang, R., Zhang, H., 2020. Detailed structure of mantle transition zone beneath southeastern China and its implications for thinning of the continental lithosphere. Tectonophysics 789, 228480. https://doi.org/10.1016/j.tecto.2020.228480.
Hao, Y.-T., Bonadiman, C., Coltorti, M., Xia, Q.-K., 2019. Fragments of asthenosphere incorporated in the lithospheric mantle underneath the Subei Basin, eastern China: Constraints from geothermobarometric results and water contents of peridotite xenoliths in Cenozoic basalts. J. Asian Earth Sci. X 1, 100006. https://doi.org/10.1016/j.jaesx.2019.100006.
Herceg, M., Artemieva, I.M., Thybo, H., 2016. Sensitivity analysis of crustal correction for calculation of lithospheric mantle density from gravity data. Geophys. J. Int. 204 (2), 738–747. https://doi.org/10.1093/gji/ggv431.
Hong, L.-B., Xu, Y.-G., Ren, Z.-Y., Kuang, Y.-S., Zhang, Y.-L., Li, J., et al., 2012. Petrology, geochemistry and Re–Os isotopes of peridotite xenoliths from Yantai, Shandong Province: evidence for Phanerozoic lithospheric mantle beneath eastern North China Craton. Lithos 155, 256–271. https://doi.org/10.1016/j.lithos.2012.09.005.
Huang, J., Zhao, D., 2006. High-resolution mantle tomography of China and surrounding regions. J. Geophys. Res. 111 (B9), B09305 https://doi.org/10.1029/2005JB004066.
Huang, Z., Gou, T., Wang, L., 2021. P and S wave tomography of east-Central China: insight into past and present mantle dynamics. Tectonophysics 809, 228859. https://doi.org/10.1016/j.tecto.2021.228859.
Jia, S., Wang, F., Tian, X., Duan, Y., Zhang, J., Liu, B., Lin, J., 2014. Crustal structure and tectonic study of North China Craton from a long deep seismic sounding profile. Tectonophysics 627, 48–56. https://doi.org/10.1016/j.tecto.2014.04.013.
Jia, Z., Meng, L.S., 2009. Some improvements on the formula for calculating the gravity anomaly due to a 2D homegeneous polygonal source. Prog. Geophys. 24 (2), 462–467 (in Chinese with abstract in English). https://doi.org/10.3969/j.issn.1004-2903.2009.02.012.
Jiang, G., Hu, S., Shi, Y., Zhang, C., Wang, Z., Hu, D., 2019. Terrestrial heat flow of continental China: updated dataset and tectonic implications. Tectonophysics 753, 36–48. https://doi.org/10.1016/j.tecto.2019.01.006.
Kiminami, K., Imaoka, T., 2013. Spatiotemporal variations of Jurassic–cretaceous magmatism in eastern Asia (Tan-Lu Fault to SW Japan): evidence for flat-slab subduction and slab rollback. Terra Nova 25 (5), 414–422. https://doi.org/10.1111/ter.12051.
King, S.D., Frost, D.J., Rubie, D.C., 2015. Why cold slabs stagnate in the transition zone. Geology 43 (3), 231–234.
Kuritani, T., Ohtani, E., Kimura, J.-I., 2011. Intensive hydration of the mantle transition zone beneath China caused by ancient slab stagnation. Nat. Geosci. 4, 713–716. https://doi.org/10.1038/ngeo1250.
Lei, J., 2012. Upper-mantle tomography and dynamics beneath the North China Craton. J. Geophys. Res. 117, B06313 https://doi.org/10.1029/2012JB009212.
Lei, J., Zhao, D., 2005. P-wave tomography and origin of the Changbai intraplate volcano in Northeast Asia. Tectonophysics 397, 281–295. https://doi.org/10.1016/j.tecto.2004.12.009.
Li, C., van der Hilst, R.D., 2010. Structure of the upper mantle and transition zone beneath Southeast Asia from traveltime tomography. J. Geophys. Res. 115 (B7) https://doi.org/10.1029/2009JB006882.
Li, H.-Y., Xu, Y.-G., Ryan, J.G., Huang, X.-L., Ren, Z.-Y., Guo, H., Ning, Z.-G., 2016. Olivine and melt inclusion chemical constraints on the source of intracontinental basalts from the eastern North China Craton: discrimination of contributions from the subducted Pacific slab. Geochim. Cosmochim. Acta 178, 1–19. https://doi.org/10.1016/j.gca.2015.12.032.
Li, H.-Y., Li, J., Ryan, J.G., Li, X., Zhao, R.-P., Ma, L., Xu, Y.-G., 2019. Molybdenum and boron isotope evidence for fluid-fluxed melting of intraplate upper mantle beneath the eastern North China Craton. Earth Planet. Sci. Lett. 520, 105–114. https://doi.org/10.1016/j.epsl.2019.05.038.
Li, J., Wang, X., Wang, X., Yuen, D.A., 2013. P and SH velocity structure in the upper mantle beneath Northeast China: evidence for a stagnant slab in hydrous mantle transition zone. Earth Planet. Sci. Lett. 367, 71–81. https://doi.org/10.1016/j.epsl.2013.02.026.
Li, Y., Gao, M., Wu, Q., 2014. Crustal thickness map of the Chinese mainland from teleseismic receiver functions. Tectonophysics 611, 51–60. https://doi.org/10.1016/j.tecto.2013.11.019.
Liu, Z., Niu, F., Chen, Y.J., Grand, S., Kawakatsu, H., Ning, J., et al., 2015a. Receiver function images of the mantle transition zone beneath NE China: new constraints on intraplate volcanism, deep subduction and their potential link. Earth Planet. Sci. Lett. 412, 101–111. https://doi.org/10.1016/j.epsl.2014.12.019.
Liu, J., Rudnick, R.L., Walker, R.J., Xu, W.-l., Gao, S., & Wu, F.-y., 2015b. Big insights from tiny peridotites: evidence for persistence of Precambrian lithosphere beneath the eastern North China Craton. Tectonophysics 650, 104–112. https://doi.org/10.1016/j.tecto.2014.05.009.
Liu, X., Zhao, D., Li, S., Wei, W., 2017. Age of the subducting Pacific slab beneath East Asia and its geodynamic implications. Earth Planet. Sci. Lett. 464, 166–174. https://doi.org/10.1016/j.epsl.2017.02.024.
Ma, X., 1989. Lithosphere and Dynamics Atlas of China. Chinese State Seismological Bureau. China Cartographic Publishing House, Beijing.
Ma, Q., Xu, Y.-G., 2021. Magmatic perspective on subduction of Paleo-Pacific plate and initiation of big mantle wedge in East Asia. Earth Sci. Rev. 213, 103473. https://doi.org/10.1016/j.earscirev.2020.103473.
Ma, Q., Xu, Y.-G., Deng, Y., Zheng, J.-P., Sun, M., Griffin, W.L., Xia, B., Wang, C.Y., 2019. Similar crust beneath disrupted and intact cratons: arguments against lower-crust delamination as a decratonization trigger. Tectonophysics 750, 1–8. https://doi.org/10.1016/j.tecto.2018.11.007.
McKenzie, D., Jackson, J., Priestley, K., 2005. Thermal structure of oceanic and continental lithosphere. Earth Planet. Sci. Lett. 233 (3), 337–349. https://doi.org/10.1016/j.epsl.2005.02.005.
Menzies, M.A., Fan, W., Zhang, M., 1993. Palaeozoic and Cenozoic lithoprobes and the loss of >120 km of Archaean lithosphere, Sino-Korean craton, China. Geol. Soc. Lond., Spec. Publ. 76 (1), 71–81. https://doi.org/10.1144/GSL.SP.1993.076.01.04.
Mooney, W.D., Kaban, M.K., 2010. The north American upper mantle: density, composition, and evolution. J. Geophys. Res. 115 (B12), B12424 https://doi.org/10.1029/2010JB000866.
Nishi, M., Kubo, T., Ohfuji, H., Kato, T., Nishihara, Y., Irifune, T., 2013. Slow Si–Al interdiffusion in garnet and stagnation of subducting slabs. Earth Planet. Sci. Lett. 361, 44–49. https://doi.org/10.1016/j.epsl.2012.11.022.
Niu, Y.L., 2005. Generation and evolution of basaltic magmas: some basic concepts and a hypothesis for the origin of the Mesozoic-Cenozoic volcanism in eastern China. Geol. J. China Univ. 11, 9–46.
Ohtani, E., Zhao, D., 2009. The role of water in the deep upper mantle and transition zone: dehydration of stagnant slabs and its effects on the big mantle wedge. Russ. Geol. Geophys. 50 (12), 1073–1078. https://doi.org/10.1016/j.rgg.2009.11.006.
Pan, S., Zheng, J., Chu, L., Griffin, W.L., 2013. Coexistence of the moderately refractory and fertile mantle beneath the eastern Central Asian Orogenic Belt. Gondwana Res 23 (1), 176–189. https://doi.org/10.1016/j.gr.2012.03.001.
Pavlis, N.K., Holmes, S.A., Kenyon, S.C., Factor, J.K., 2012. The development and evaluation of the Earth Gravitational Model 2008 (EGM2008). J. Geophys. Res. 117 (B4), B04406 https://doi.org/10.1029/2011JB008916.
Polat, A., Herzberg, C., Munker, C., Rodgers, R., Kusky, T., Li, J., et al., 2006. Geochemical and petrological evidence for a suprasubduction zone origin of Neoarchean (ca. 2.5 Ga) peridotites, central orogenic belt, North China craton. Geol. Soc. Am. Bull. 118 (7–8), 771–784. https://doi.org/10.1130/B25845.1.
Schutt, D.L., Lesher, C.E., 2010. Compositional trends among Kaapvaal Craton garnet peridotite xenoliths and their effects on seismic velocity and density. Earth Planet. Sci. Lett. 300 (3), 367–373. https://doi.org/10.1016/j.epsl.2010.10.018.
Sun, M., Gao, S.S., Liu, K.H., Fu, X., 2020. Upper mantle and mantle transition zone thermal and water content anomalies beneath NE Asia: Constraints from receiver function imaging of the 410 and 660 km discontinuities. Earth Planet. Sci. Lett. 532, 116040. https://doi.org/10.1016/j.epsl.2019.116040.
Sun, P., Guo, P., Niu, Y., 2021. Eastern China continental lithosphere thinning is a consequence of paleo-Pacific plate subduction: A review and new perspectives. Earth Sci. Rev. 218, 103680. https://doi.org/10.1016/j.earscirev.2021.103680.
Sun, Y., Dong, S., Zhang, H., Li, H., Shi, Y., 2013. 3D thermal structure of the continental lithosphere beneath China and adjacent regions. J. Asian Earth Sci. 62, 697–704. https://doi.org/10.1016/j.jseaes.2012.11.020.
Tian, X., Zelt, C.A., Wang, F., Jia, S., Liu, Q., 2014. Crust structure of the North China Craton from a long-range seismic wide-angle-reflection/refraction data. Tectonophysics 634, 237–245. https://doi.org/10.1016/j.tecto.2014.07.008.

Vinnik, L., Deng, Y., Kosarev, G., Oreshin, S., Zhang, Z., Makeyeva, L., 2020. Sharpness of the 410-km discontinuity from the P410s and P2p410s seismic phases. Geophys. J. Int. 220, 1208–1214. https://doi.org/10.1093/gji/ggz507.

Wang, H., 1985. Atlas of the Palaeogeography of China. Cartographic Publishing House, Beijing.

Wang, S., Wang, F., Zhang, J., Jia, S., Zhang, C., Zhao, J., Liu, B., 2014. The P-wave velocity structure of the lithosphere of the North China Craton—results from the Wendeng-Alxa Left Banner deep seismic sounding profile. Sci. China Earth Sci. 57 (9), 2053–2063. https://doi.org/10.1007/s11430-014-4903-7.

Wang, X., Chen, Q.-F., Niu, F., Wei, S., Ning, J., Li, J., et al., 2020. Distinct slab interfaces imaged within the mantle transition zone. Nat. Geosci. 13, 822–827. https://doi.org/10.1038/s41561-020-00653-5.

Wang, X.J., Chen, L.H., Hofmann, A.W., Mao, F.G., Liu, J.Q., Zhong, Y., Xie, L.W., Yang, Y.H., 2017. Mantle transition zone-derived EM1 component beneath NE China: Geochemical evidence from Cenozoic potassic basalts. Earth Planet. Sci. Lett. 465, 16–28. https://doi.org/10.1016/j.epsl.2017.02.028.

Wei, W., Zhao, D., Xu, J., Wei, F., Liu, G., 2015. P and S wave tomography and anisotropy in Northwest Pacific and East Asia: constraints on stagnant slab and intraplate volcanism. J. Geophys. Res. 120, 1642–1666. https://doi.org/10.1002/2014JB011254.

Wu, F.Y., Xu, Y.G., Gao, S., Zheng, J.P., 2008. Lithospheric thinning and destruction of the North China Craton. Acta Petrologica Sinica (in Chinese with English abstract) 24 (6), 1145–1174.

Wu, F.-Y., Yang, J.-H., Xu, Y.-G., Wilde, S.A., Walker, R.J., 2019. Destruction of the North China Craton in the Mesozoic. Annu. Rev. Earth Planet. Sci. 47 (1), 173–195. https://doi.org/10.1146/annurev-earth-053018-060342.

Xia, Q.-K., Liu, J., Kovács, I., Hao, Y.-T., Li, P., Yang, X.-Z., et al., 2019. Water in the upper mantle and deep crust of eastern China: concentration, distribution and implications. Natl. Sci. Rev. 6 (1), 125–144. https://doi.org/10.1093/nsr/nwx016.

Xiao, Y., Zhang, H.-F., Fan, W.-M., Ying, J.-F., Zhang, J., Zhao, X.-M., Su, B.-X., 2010. Evolution of lithospheric mantle beneath the Tan-Lu fault zone, eastern North China Craton: evidence from petrology and geochemistry of peridotite xenoliths. Lithos 117 (1), 229–246. https://doi.org/10.1016/j.lithos.2010.02.017.

Xu, Q., Liu, J., He, H., Zhang, Y., 2019. Nature and evolution of the lithospheric mantle revealed by water contents and He-Ar isotopes of peridotite xenoliths from Changbaishan and Longgang basalts in Northeast China. Sci. Bull. 64 (18), 1325–1335. https://doi.org/10.1016/j.scib.2019.07.006.

Xu, W., Yang, D., Gao, S., Pei, F., Yu, Y., 2010a. Geochemistry of peridotite xenoliths in Early Cretaceous high-Mg# diorites from the Central Orogenic Block of the North China Craton: the nature of Mesozoic lithospheric mantle and constraints on lithospheric thinning. Chem. Geol. 270 (1), 257–273. https://doi.org/10.1016/j.chemgeo.2009.12.006.

Xu, W., Wang, C., Yang, D., Wang, F., Pei, F., 2010b. Dunite xenoliths and olivine xenocrysts in gabbro from Taihang Mountains: characteristics of Mesozoic lithospheric mantle in Central China. J. Earth Sci. 21 (5), 692–710. https://doi.org/10.1007/s12583-010-0121-1.

Xu, Y., Li, H., Hong, L., Ma, L., Ma, Q., Sun, M., 2018. Generation of Cenozoic intraplate basalts in the big mantle wedge under eastern Asia. Sci. China Earth Sci. 61 (7), 869–886. https://doi.org/10.1007/s11430-017-9192-y.

Xu, Y.G., 2001. Thermo-tectonic destruction of the Archaean lithospheric keel beneath eastern China: evidence, timing and mechanism. Phys. Chem. Earth 26, 747–757. https://doi.org/10.1016/S1464-1895(01)00124-7.

Xu, Y.G., 2007. Diachronous lithospheric thinning of the North China Craton and formation of the Daxin'anling-Taihangshan gravity lineament. Lithos 96, 281–298. https://doi.org/10.1016/j.lithos.2006.09.013.

Xu, Y.-G., Blusztajn, J., Ma, J.-L., Suzuki, K., Liu, J.F., Hart, S.R., 2008. Late Archean to early Proterozoic lithospheric mantle beneath the western North China craton: Sr–Nd–Os isotopes of peridotite xenoliths from Yangyuan and Fansi. Lithos 102 (1), 25–42. https://doi.org/10.1016/j.lithos.2007.04.005.

Xu, Y.-G., Zhang, H.-H., Qiu, H.-N., Ge, W.-C., Wu, F.-Y., 2012. Oceanic crust components in continental basalts from Shuangliao, Northeast China: derived from the mantle transition zone? Chem. Geol. 328, 168–184. https://doi.org/10.1016/j.chemgeo.2012.01.027.

Zhang, B., Lei, J., Yuan, X., Zhang, G., He, J., Xu, Q., 2020. Detailed Moho variations under Northeast China inferred from receiver function analyses and their tectonic implications. Phys. Earth Planet. Inter. 300, 106448. https://doi.org/10.1016/j.pepi.2020.106448.

Zhang, H., Liu, J., Santosh, M., Tao, N., Zhou, Q., Hu, B., 2017. Ultra-depleted peridotite xenoliths in the Northern Taihang Mountains: implications for the nature of the lithospheric mantle beneath the North China Craton. Gondwana Res. 48, 72–85. https://doi.org/10.1016/j.gr.2017.04.009.

Zhang, H., Zhang, H., Zou, D., 2021. Comprehensive refertilization of the Archean–Paleoproterozoic lithospheric mantle beneath the northwestern North China Craton: evidence from in situ Sr isotopes of the Siziwangqi peridotites. Lithos 380-381, 105822. https://doi.org/10.1016/j.lithos.2020.105822.

Zhang, H.-F., 2005. Transformation of lithospheric mantle through peridotite-melt reaction: A case of Sino-Korean craton. Earth Planet. Sci. Lett. 237 (3–4), 768–780. https://doi.org/10.1016/j.epsl.2005.06.041.

Zhang, R., Wu, Q., Sun, L., He, J., Gao, Z., 2014. Crustal and lithospheric structure of Northeast China from S-wave receiver functions. Earth Planet. Sci. Lett. 401, 196–205. https://doi.org/10.1016/j.epsl.2014.06.017.

Zhang, Y.Y., Chen, L., Ai, Y.S., Jiang, M.M., Xu, W.W., Shen, Z.Y., 2018. Lithospheric structure of the South China block from S-receiver function. Chin. J. Geophys. 61 (1), 138–149. https://doi.org/10.6038/cjg2018L0226.

Zhao, D., 2004. Global tomographic images of mantle plumes and subducting slabs: insight into deep Earth dynamics. Phys. Earth Planet. Inter. 146, 3–34. https://doi.org/10.1016/j.pepi.2003.07.032.

Zhao, D., Lei, J., Tang, R., 2004. Origin of the Changbai intraplate volcanism in Northeast China: evidence from seismic tomography. Chin. Sci. Bull. 49 (13), 1401–1408. https://doi.org/10.1360/04wd0125.

Zhao, D., Maruyama, S., Omori, S., 2007. Mantle dynamics of Western Pacific and East Asia: insight from seismic tomography and mineral physics. Gondwana Res. 11, 120–131. https://doi.org/10.1016/j.gr.2006.06.006.

Zhao, X., Wang, H., Li, Z., Evans, N.J., Ying, J., Yang, Y., Zhang, H., 2021. Nature and evolution of lithospheric mantle beneath the western North China Craton: constraints from peridotite and pyroxenite xenoliths in the Sanyitang basalts. Lithos 384-385, 105987. https://doi.org/10.1016/j.lithos.2021.105987.

Zheng, J., Griffin, W., O'Reilly, S.Y., Yu, C., Zhang, H., Pearson, N., Zhang, M., 2007. Mechanism and timing of lithospheric modification and replacement beneath the eastern North China Craton: peridotitic xenoliths from the 100 Ma Fuxin basalts and a regional synthesis. Geochim. Cosmochim. Acta 71 (21), 5203–5225. https://doi.org/10.1016/j.gca.2007.07.028.

Zheng, T.Y., Zhao, L., Chen, L., 2005. A detailed receiver function image of the sedimentary structure in the Bohai Bay Basin. Phys. Earth Planet. Inter. 152, 129–143. https://doi.org/10.1016/j.pepi.2005.06.011.

Zheng, T.-Y., Zhao, L., He, Y.-M., Zhu, R.-X., 2014. Seismic imaging of crustal reworking and lithospheric modification in eastern China. Geophys. J. Int. 196 (2), 656–670. https://doi.org/10.1093/gji/ggt420.

Zhu, G., Jiang, D., Zhang, B., Chen, Y., 2012a. Destruction of the eastern North China Craton in a backarc setting: evidence from crustal deformation kinematics. Gondwana Res. 22 (1), 86–103. https://doi.org/10.1016/j.gr.2011.08.005.

Zhu, R., Xu, Y., Zhu, G., Zhang, H., Xia, Q., Zheng, T., 2012b. Destruction of the North China Craton. Sci. China Earth Sci. 55 (10), 1565–1587. https://doi.org/10.1007/s11430-012-4516-y.

Zou, D., Zhang, H., Hu, Z., Santosh, M., 2016. Complex metasomatism of lithospheric mantle by asthenosphere-derived melts: evidence from peridotite xenoliths in Weichang at the northern margin of the North China Craton. Lithos 264, 210–223. https://doi.org/10.1016/j.lithos.2016.08.036.